

## Research Article

# Double Magnetic Loop and Methods for Calculating Its Inductance

**Ferran Mocholí Belenguer** <sup>1</sup>, **Antonio Mocholí Salcedo**,<sup>2</sup>  
**Victor Milián Sánchez**,<sup>3</sup> and **José Humberto Arroyo Núñez**<sup>4</sup>

<sup>1</sup>Traffic Control Systems Group, ITACA Institute, Universitat Politècnica de València, Valencia 46022, Spain

<sup>2</sup>Department of Electronic Engineering, ITACA Institute, Universitat Politècnica de València, Valencia 46022, Spain

<sup>3</sup>Chemical and Nuclear Engineering Department, Institute of Industrial, Radiological and Environmental Safety, Universitat Politècnica de València, Valencia 46022, Spain

<sup>4</sup>Electronic and Telecommunications Engineering Department, Universidad Politécnica de Tulancingo, Tulancingo 43629, Mexico

Correspondence should be addressed to Ferran Mocholí Belenguer; fermocbe@upv.es

Received 12 June 2018; Accepted 6 September 2018; Published 25 September 2018

Guest Editor: Darius Andriukaitis

Copyright © 2018 Ferran Mocholí Belenguer et al. This is an open access article distributed under the Creative Commons Attribution License, which permits unrestricted use, distribution, and reproduction in any medium, provided the original work is properly cited.

Due to their simplicity and operating mode, magnetic loops are one of the most used traffic sensors in Intelligent Transportation Systems (ITS). However, at this moment, their potential is not being fully exploited, as neither the speed nor the length of the vehicles can be surely ascertained with the use of a single magnetic loop. In this way, the vast majority of them are only being used to count vehicles on urban and interurban roads. For this reason, in order to contribute to the development of new traffic sensors and make roads safer, this paper introduces a theoretical study to explain the design and peculiarities of the innovative double loops, how to calculate their magnetic field and three different methods to calculate their inductance. Finally, the different inductance values obtained by these three methods will be analyzed and compared with experimental measurements carried out by our research group in order to know which method is more accurate and if all of them are equally reliable.

## 1. Introduction

Magnetic loops are the most common sensors on roads around the world since they are an affordable and highly developed technology with a simple operation that is not affected by environmental conditions [1–7]. Although these ones imply to drill and work on the road for their installation and possible future repairs like the rest of intrusive sensors [8], in practice, magnetic loops still have a long future ahead. Even though they might seem outdated, these are actually a widely extended and well-known reliable technology that offers good performance at a low price. Proof of this is that today they continue to be installed on the roads and they are even fundamental elements in the new algorithms for traffic management [9–15].

Their operation is straightforward, since it is based on the impedance variation that is recorded in the magnetic loops

during the passage of vehicles over them, and as shown in Figure 1, an entire system usually consists of three parts [16]:

- (I) A magnetic loop formed by a wire with one or more turns superficially buried in the pavement.
- (II) A cable that links the magnetic loop with the control booth, which is also buried in the pavement.
- (III) An electronic unit located in the control booth that contains an oscillator and amplifiers to excite the inductive loop.

In order to have a better understanding of how they work, there are many publications and bibliography [1] since they are one of the most widespread sensors. However, a brief physical explanation is provided in the following points:

- (i) The electronic unit together with the magnetic loop forms an oscillator circuit.

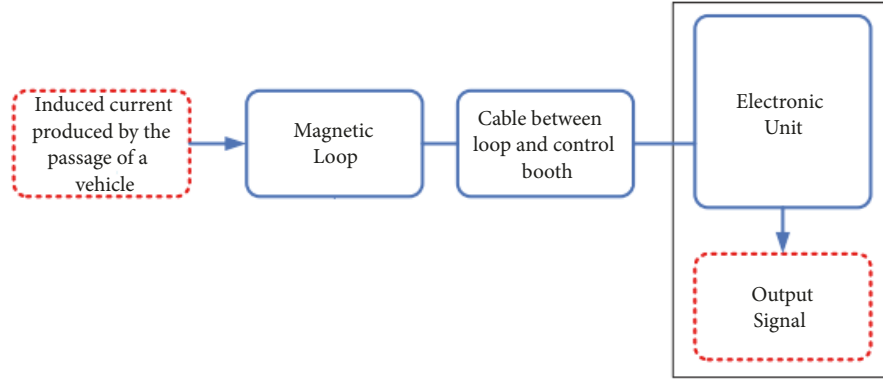


FIGURE 1: Magnetic loop system scheme.

- (ii) The current which passes through the loop produces a magnetic field  $\vec{H}$  around the cable as shown in (1), where  $N$  is the number of turns of the loop,  $I$  is the current expressed in Amperes, and  $l$  is the length of the loop expressed in meters.

$$\vec{H} = \frac{N \cdot I}{l} \quad (1)$$

- (iii) This magnetic field  $\vec{H}$  produces a magnetic flux  $\emptyset$  through the loop as shown in (2), where  $\vec{B}$  is the magnetic flux density,  $\vec{S}$  is the surface enclosed by the loop,  $\mu_r$  is the relative magnetic permeability of the medium, and  $\mu_o$  is a constant value ( $4\pi \cdot 10^{-7} \text{ N / A}^2$ ).

$$\emptyset = \vec{B} \cdot \vec{S} = \mu_r \cdot \mu_o \cdot \vec{H} \cdot \vec{S} \quad (2)$$

- (iv) The result is that the inductance of a common single loop  $L$  expressed in Henrys is obtained as follows:

$$L = \frac{N \cdot \emptyset}{I} = \frac{N \cdot \vec{B} \cdot \vec{S}}{I} \quad (3)$$

In this way, when a vehicle or any object built with ferromagnetic materials passes through the magnetic field generated by a magnetic loop buried on the road with a surface area  $\vec{S}$ , a number of turns  $N$ , and a current intensity  $I$  as shown in Figure 2, there is a decrease in the global magnetic field because of the currents that are induced in the vehicle.

As seen in (3), the loop inductance is proportional to the magnetic flux, which causes that when passing a vehicle over it, the inductance also decreases. Moreover, like any oscillator circuit, the oscillation frequency of the whole system will be given by

$$f = \frac{k}{L} \quad (4)$$

where  $k$  is a constant that depends on the characteristics of the electronic components used in the construction of the

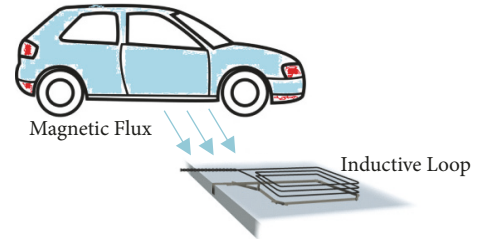


FIGURE 2: Magnetic loop operation mode.

oscillator circuit. Thus, when a vehicle passes over a loop, we can obtain what is commonly known as “the vehicle magnetic profile” or “the vehicle inductance signature” by analyzing the inductance or frequency variation recorded. This magnetic profile is different for each type of vehicle as seen in Figure 3, which allows classifying the different vehicles as motorcycles, cars, trucks and buses. However, while the vehicle magnetic profiles for the single loops are widely known, the magnetic profiles left by the passage of vehicles over the double loops have not yet been studied, although we can anticipate that these new magnetic profiles will offer much more information than the previous ones.

To estimate the vehicle speed and classify them, nowadays it is necessary to use two single loops, since a single one is not able to get all the necessary parameters to do it. After analyzing the magnetic profile, there are two unknown data (vehicle length and vehicle speed) with the variation of a single parameter (inductance or oscillation frequency).

For that reason, there are usually two loops per lane separated by a certain distance. In this manner, the passage of a vehicle over the first loop is recorded in the detector, and after a short interval of time, the vehicle passes again over the second loop where it is also recorded [8, 17]. Then, as the distance between both loops is known by design, the vehicle speed, the direction of traffic and the vehicle length can be finally estimated, as well as the vehicle axle detection [14].

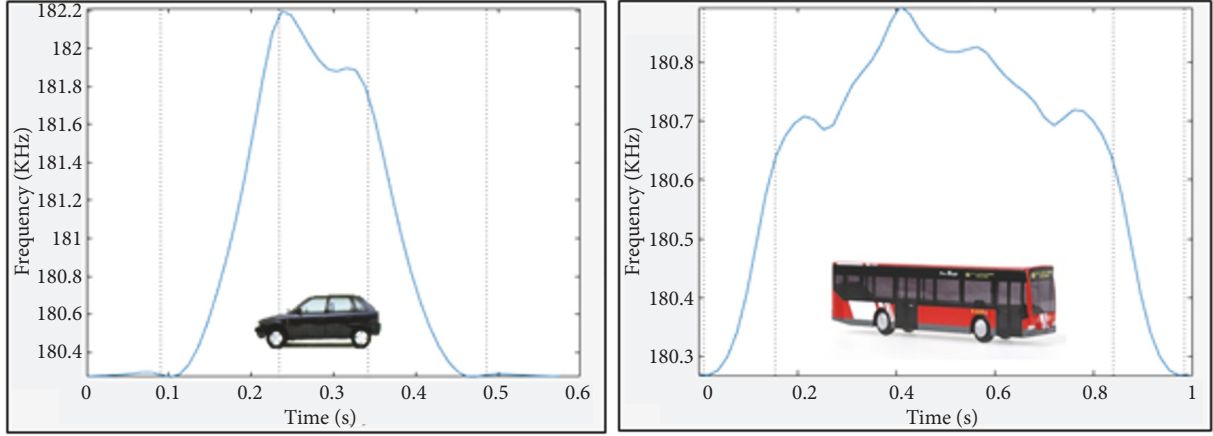


FIGURE 3: Magnetic profiles. (a) Car. (b) Bus.

Nevertheless, with the use of the double loops this problem would be solved and it would only be necessary to use one loop to find out all the previous data, since they have a simpler, more compact and more economical electronics. Moreover, having a single signal instead of two would facilitate the implementation of the measurement system.

Therefore, our work will aim to present and describe the characteristics of the double loop, to offer different methods to calculate its inductance, to verify which one provides better results and to improve the functional characteristics of the popular single loops, which despite being the most installed sensor on the roads, they are actually only dedicated to count vehicles. The presentation of the new vehicle magnetic profiles, the parameters that can be extracted with them and the advantages offered over the conventional loop will be the subject of the following paper.

## 2. Electromagnetic Analysis

The design, shape, and construction of a rectangular or circular single loop are well-known worldwide [3]. However, although every day there are more algorithms and new systems to regulate traffic based on magnetic loops [18, 19], the double loop capable of providing better performance than the current loops at lower cost is still unknown.

A double loop is no more than the union of two rectangular loops, which can have different dimensions and turns (not to be confused with two single loops spaced at a certain distance as described above). How to implement this type of loop can be quite varied, but a classic way to proceed would be to build the outer loop and then a smaller inner loop located at one extreme. However, another way to build it could be to construct a small loop and then put another small one next to the first one. In all cases, the direction of the current in each loop can be chosen with the aim of generating different types of configurations. At any rate, in our study we will present a general theoretical analysis capable of simulating any type of design. Therefore, in order to analyze this type of loop, the space will be divided into three sections as shown in Figure 4.

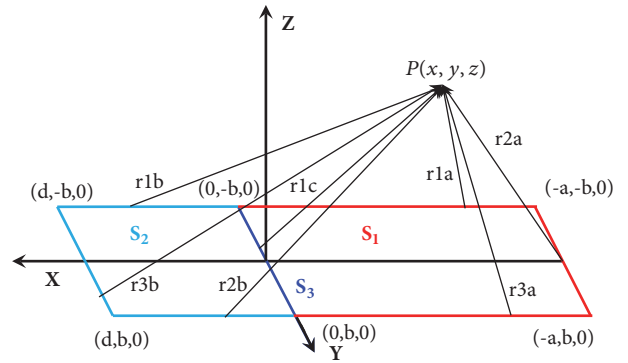


FIGURE 4: Double loop presented in three sections.

- (i) The first section,  $S_1$ , corresponds to the three red segments located in the plane of the negative values of  $X$ . Two segments parallel to the  $X$ -axis with a length of  $a$  and one segment parallel to the  $Y$ -axis with a length of  $2b$ .
- (ii) The second section,  $S_2$ , corresponds to the three turquoise segments located in the plane of the positive values of  $X$ . Two segments parallel to the  $X$ -axis with a length of  $d$  and one segment parallel to the  $Y$ -axis with a length of  $2b$ .
- (iii) The third section,  $S_3$ , corresponds to the blue segment located on the  $Y$ -axis at  $X = 0$  which has a length of  $2b$ .

In this way, point  $P$  where the magnetic field will be calculated will be determined by its coordinates  $(x, y, z)$ . Consequently and as shown in Figure 4, the distances from any point of the double loop  $(x', y', z')$  to the point of analysis of the magnetic field  $P(x, y, z)$  will be defined as follows:

$$r1a = \sqrt{(x - x')^2 + (y + b)^2 + z^2}$$

$$r2a = \sqrt{(x + a)^2 + (y - y')^2 + z^2}$$

$$\begin{aligned}
r3a &= \sqrt{(x-x')^2 + (y-b)^2 + z^2} \\
r1b &= \sqrt{(x-x')^2 + (y+b)^2 + z^2} \\
r2b &= \sqrt{(x-x')^2 + (y-b)^2 + z^2} \\
r3b &= \sqrt{(x-d)^2 + (y-y')^2 + z^2} \\
r1c &= \sqrt{x^2 + (y-y')^2 + z^2}
\end{aligned} \tag{5}$$

In order to perform the electromagnetic analysis, the starting point will be the physical phenomenon of magnetic field generation due to the electrical currents flowing through a conductor. Maxwell's equations [20] revealed that the divergence of  $\vec{B}$  is zero:

$$\vec{\nabla} \cdot \vec{B} = 0 \tag{6}$$

This indicates that  $\vec{B}$  has the solenoidal property (with no divergence), which means that the magnetic field  $\vec{B}$  can be represented using an auxiliary vector function  $\vec{A}$  as follows:

$$\vec{B} = \vec{\nabla} \times \vec{A} \tag{7}$$

And thus

$$\vec{\nabla} \cdot (\vec{\nabla} \times \vec{A}) = 0 \tag{8}$$

The auxiliary vector  $\vec{A}$  is called magnetic potential vector [21] and it is related to the sources of the stable current density  $J$  which are responsible for generating the magnetic field. Then, in the case of a linear conductor,  $\vec{A}$  is given by

$$\vec{A} = \int_l \frac{\mu_0 I d\vec{l}}{4\pi r} \tag{9}$$

where  $I$  is the current in the linear conductor and  $r$  is the distance from the conductor to the analysis point. However, (9) represents a solution for the case of thin conductors, but the general solution must include a volumetric integral. In this way, the magnetic potential vector for each segment of our inductive double loop is obtained as follows:

Section  $S_1$

$$\begin{aligned}
\vec{A}_{1s1x} &= \frac{\mu_0 I}{4\pi} \ln \frac{\sqrt{(x+a)^2 + (y+b)^2 + z^2} - a - x}{\sqrt{x^2 + (y+b)^2 + z^2} - x} \\
\vec{A}_{2s1y} &= \frac{\mu_0 I}{4\pi} \ln \frac{\sqrt{(x+a)^2 + (y-b)^2 + z^2} + b - y}{\sqrt{(x+a)^2 + (y+b)^2 + z^2} - b - y} \\
\vec{A}_{3s1x} &= \frac{\mu_0 I}{4\pi} \ln \frac{\sqrt{x^2 + (y-b)^2 + z^2} - x}{\sqrt{(x+a)^2 + (y-b)^2 + z^2} - a - x}
\end{aligned} \tag{10a}$$

Section  $S_2$

$$\begin{aligned}
\vec{A}_{1s2x} &= \frac{\mu_0 I}{4\pi} \ln \frac{\sqrt{x^2 + (y+b)^2 + z^2} - x}{\sqrt{(x-d)^2 + (y+b)^2 + z^2} + d - x} \\
\vec{A}_{2s2x} &= \frac{\mu_0 I}{4\pi} \ln \frac{\sqrt{(x-d)^2 + (y-b)^2 + z^2} + d - x}{\sqrt{x^2 + (y-b)^2 + z^2} - x} \\
\vec{A}_{3s2y} &= \frac{\mu_0 I}{4\pi} \ln \frac{\sqrt{(x-d)^2 + (y+b)^2 + z^2} - b - y}{\sqrt{(x-d)^2 + (y-b)^2 + z^2} + b - y}
\end{aligned} \tag{10b}$$

Section  $S_3$

$$\vec{A}_{1s3y} = \frac{\mu_0 I}{4\pi} \ln \frac{\sqrt{x^2 + (y-b)^2 + z^2} + b - y}{\sqrt{x^2 + (y+b)^2 + z^2} - b - y} \tag{10c}$$

In the previous expressions ( $A_{isjk}$ ) it must be noted that, as shown in Figure 4, the subindex  $i$  refers to the considered segment of the section  $sj$ , which in turn corresponds to the  $k$ -axis. For example,  $\vec{A}_{3s2y}$  would mean the third segment of section  $S_2$  located on the  $Y$ -axis, and the values  $a$ ,  $b$  and  $d$  would correspond to the dimensions of the loop described above. However, before proceeding with the electromagnetic analysis of the double loop, we will define a series of terms to simplify the previous equations. These terms will be

$$\begin{aligned}
R_1 &= \sqrt{x^2 + (y+b)^2 + z^2} \\
R_2 &= \sqrt{(x-d)^2 + (y+b)^2 + z^2} \\
R_3 &= \sqrt{x^2 + (y-b)^2 + z^2} \\
R_4 &= \sqrt{(x-d)^2 + (y-b)^2 + z^2} \\
R_{1a} &= \sqrt{(x+a)^2 + (y+b)^2 + z^2} \\
R_{2a} &= R_1 \\
R_{3a} &= \sqrt{(x+a)^2 + (y-b)^2 + z^2} \\
R_{4a} &= R_3 \\
c_1 &= -x \\
c_2 &= d - x \\
d_1 &= -b - y \\
d_2 &= b - y \\
c_{1a} &= -a - x \\
c_{2a} &= c_1 \\
d_{1a} &= d_1 \\
d_{2a} &= d_2
\end{aligned} \tag{11}$$

In this way, combining (10a), (10b), and (10c) with (11), we can obtain the magnetic potentials vectors in a simpler way as seen in the following:

$$\begin{aligned}
\vec{A}_{1s1x} &= \frac{\mu_0 I}{4\pi} \ln \frac{R_{1a} + c_{1a}}{R_{2a} + c_{2a}} \\
\vec{A}_{2s1y} &= \frac{\mu_0 I}{4\pi} \ln \frac{R_{3a} + d_{2a}}{R_{1a} + d_{1a}} \\
\vec{A}_{3s1x} &= \frac{\mu_0 I}{4\pi} \ln \frac{R_{4a} + c_{2a}}{R_{3a} + c_{1a}} \\
\vec{A}_{1s2x} &= \frac{\mu_0 I}{4\pi} \ln \frac{R_1 + c_1}{R_2 + c_2} \\
\vec{A}_{2s2x} &= \frac{\mu_0 I}{4\pi} \ln \frac{R_4 + c_2}{R_3 + c_1} \\
\vec{A}_{3s2y} &= \frac{\mu_0 I}{4\pi} \ln \frac{R_2 + d_1}{R_4 + d_2} \\
\vec{A}_{1s3y} &= \frac{\mu_0 I}{4\pi} \ln \frac{R_{4a} + d_{2a}}{R_{2a} + d_{1a}}
\end{aligned} \tag{12}$$

For the section  $S_1$ , located in the plane of the negative values of  $X$ , the magnetic potential vector would have two components,  $\hat{x}$  and  $\hat{y}$ :

$$\vec{A}_{s1} = (\vec{A}_{1s1x} + \vec{A}_{3s1x}) \hat{x} + (\vec{A}_{2s1y}) \hat{y} \tag{13}$$

For the section  $S_2$ , located in the plane of the positive values of  $X$ , the magnetic potential vector would also have two components,  $\hat{x}$  and  $\hat{y}$ :

$$\vec{A}_{s2} = (\vec{A}_{1s2x} + \vec{A}_{2s2x}) \hat{x} + (\vec{A}_{3s2y}) \hat{y} \tag{14}$$

Nevertheless, in the case of the section  $S_3$ , located on the axis  $Y$  at  $X = 0$ , it would only have component  $\hat{y}$ :

$$\vec{A}_{s3} = (\vec{A}_{1s3y}) \hat{y} \tag{15}$$

Thus, once the magnetic potential vector has been calculated, the magnetic field could already be obtained by applying the curl to the magnetic potential vector in the same way as (7). However, with the aim of obtaining the total magnetic field, the calculation must be performed for each loop section. In this manner, the equations of the three sections are presented in (16), (17), and (18) respectively.

#### Section $S_1$ –Negative Values of $X$

$$\begin{aligned}
\vec{B}_{s1x} &= \frac{\mu_0 I}{4\pi} \left[ \frac{z}{R_{1a}(R_{1a} + d_{1a})} - \frac{z}{R_{3a}(R_{3a} + d_{2a})} \right] \\
\vec{B}_{s1y} &= \frac{\mu_0 I}{4\pi} \left[ \frac{z}{R_{1a}(R_{1a} + c_{1a})} - \frac{z}{R_{2a}(R_{2a} + c_{2a})} \right. \\
&\quad \left. - \frac{z}{R_{3a}(R_{3a} + c_{1a})} + \frac{z}{R_{4a}(R_{4a} + c_{2a})} \right]
\end{aligned}$$

$$\begin{aligned}
\vec{B}_{s1z} &= \frac{\mu_0 I}{4\pi} \left[ \left( \frac{-(x+a)}{R_{1a}(R_{1a} + d_{1a})} + \frac{(x+a)}{R_{3a}(R_{3a} + d_{2a})} \right) \right. \\
&\quad \left. - \left( \frac{(y+b)}{R_{1a}(R_{1a} + c_{1a})} - \frac{(y+b)}{R_{2a}(R_{2a} + c_{2a})} \right) \right. \\
&\quad \left. - \frac{(y-b)}{R_{3a}(R_{3a} + c_{1a})} + \frac{(y-b)}{R_{4a}(R_{4a} + c_{2a})} \right]
\end{aligned} \tag{16}$$

#### Section $S_2$ –Positive Values of $X$

$$\begin{aligned}
\vec{B}_{s2x} &= \frac{\mu_0 I}{4\pi} \left[ \frac{-z}{R_2(R_2 + d_1)} - \frac{z}{R_4(R_4 + d_2)} \right] \\
\vec{B}_{s2y} &= \frac{\mu_0 I}{4\pi} \left[ \frac{z}{R_1(R_1 + c_1)} - \frac{z}{R_2(R_2 + c_2)} \right. \\
&\quad \left. - \frac{z}{R_3(R_3 + c_1)} + \frac{z}{R_4(R_4 + c_2)} \right] \\
\vec{B}_{s2z} &= \frac{\mu_0 I}{4\pi} \left[ \left( \frac{(x-d)}{R_2(R_2 + d_1)} - \frac{(x-d)}{R_4(R_4 + d_2)} \right) \right. \\
&\quad \left. - \left( \frac{(y+b)}{R_1(R_1 + c_1)} - \frac{(y+b)}{R_2(R_2 + c_2)} - \frac{(y-b)}{R_3(R_3 + c_1)} \right) \right. \\
&\quad \left. + \frac{(y-b)}{R_4(R_4 + c_2)} \right]
\end{aligned} \tag{17}$$

#### Section $S_3$ –Axis $Y$ at $X = 0$

$$\begin{aligned}
\vec{B}_{s3x} &= \frac{\mu_0 I}{4\pi} \left[ \frac{z}{R_{2a}(R_{2a} + d_{1a})} - \frac{z}{R_{4a}(R_{4a} + d_{2a})} \right] \\
\vec{B}_{s3z} &= \frac{\mu_0 I}{4\pi} \left[ \frac{x}{R_{4a}(R_{4a} + d_{2a})} - \frac{x}{R_{2a}(R_{2a} + d_{1a})} \right]
\end{aligned} \tag{18}$$

Hence, all this double loop electromagnetic analysis have led us to the conclusion that the total magnetic field produced by a double loop of dimensions  $a$ ,  $d$  and  $2b$  at a certain point  $P(x, y, z)$  as shown in Figure 4 will be the sum of the components obtained in (16), (17), and (18). The resulting expression is shown in the following:

$$\begin{aligned}
\vec{B} &= (\vec{B}_{s1x} + \vec{B}_{s2x} + \vec{B}_{s3x}) \hat{x} + (\vec{B}_{s1y} + \vec{B}_{s2y}) \hat{y} \\
&\quad + (\vec{B}_{s1z} + \vec{B}_{s2z} + \vec{B}_{s3z}) \hat{z}
\end{aligned} \tag{19}$$

### 3. Experimental Measurements

After obtaining the expression that describes the magnetic field generated by a double loop, the next step was to verify that the theoretical results coincided with the experimental ones. For this reason, a double loop was constructed in the laboratory by our research team (Group of Traffic Control

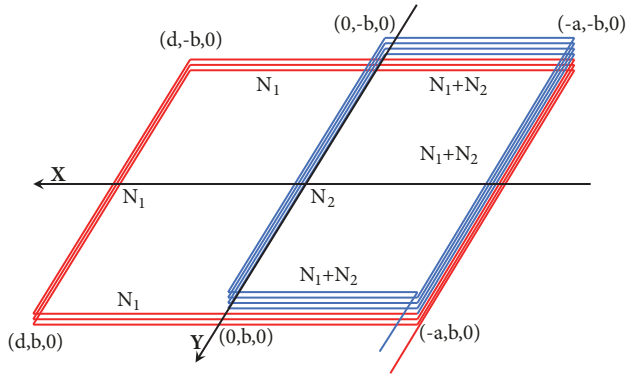


FIGURE 5: Outline of the double loop constructed.

System, ITACA Institute, Universitat Politècnica de València, Spain). It was implemented with an external loop of  $N_1$  turns and, inside and over it, a smaller one of  $N_2$  turns located in the negative half-plane, both with the same direction of circulation. The scheme is shown in Figure 5.

With these conditions, we only were interested in the component of the magnetic field perpendicular to the surface of the loop ( $\vec{B}_k$ ), as the surface vector of the loop only has component along the Z-axis. Then, taking into account the turns of each of the loop sections, this value was easily obtained from (19) as follows:

$$\vec{B}_k = (N_1 + N_2) \cdot \vec{B}_{s1z} + N_1 \cdot \vec{B}_{s2z} - N_2 \cdot \vec{B}_{s3z} \quad (20)$$

**3.1. Characteristics of the Double Loop Constructed.** Conductor type is tinned copper wire conductors individually insulated with polyvinyl chloride with a cross section of  $0.28 \text{ mm}^2$ .

Number of turns is 4 exterior turns ( $N_1$ ) of  $1.20 \times 0.46 \text{ m}$  and 5 interior turns ( $N_2$ ) of  $0.40 \times 0.46 \text{ m}$ .

Dimensions is  $1.20 \times 0.46 \text{ m}$ .

With these values, the parameters of the loop according to the nomenclature used in Figures 4 and 5 would be as follows:

$$\begin{aligned} a &= 0.40\text{m} \\ b &= 0.23\text{m} \\ d &= 0.80\text{m} \end{aligned} \quad (21)$$

**3.2. Characteristics of the Signal Used to Energize the Loop.** Frequency of the signal applied to the loop is  $139.2 \text{ kHz}$ .

Signal type is rectangular.

Current intensity through the loop (RMS) is  $51.80 \text{ mA}$ .

**3.3. Region Where the Readings of the Magnetic Field Were Carried Out.** Height above the plane of the loop is  $0.0825 \text{ m}$ . Position is along the X-axis in the center of the loop ( $Y = 0$ ).

With the above-mentioned characteristics, the theoretical calculation in the region of the measurements was carried out by applying and programming the expression obtained in



FIGURE 6: Exposure Level Tester ELT-400.



FIGURE 7: ELT-400 configuration.

(20) in Matlab ©, while the experimental measurements were performed in our laboratory in order to verify the goodness of the theoretical model developed for the calculation of the double loop magnetic field. The instrument used to measure this magnetic field was the Exposure Level Tester ELT-400 shown in Figure 6.

This device contains a series of turns with a diameter of  $0.125 \text{ m}$  and measures the magnetic field by means of this spherical sensor. It is able to detect frequencies from  $1 \text{ Hz}$  to  $400 \text{ kHz}$ , although this can be set as wished. To perform the measurements, the ELT-400 was configured as shown in Figure 7 and as follows:

Selected frequency range:  $30 \text{ Hz} - 400 \text{ kHz}$ .

Reading range:  $320 \mu\text{T}$ .

RMS signal value.

After collecting and processing all the information, the comparison between the calculated and measured values of the magnetic field as well as the tolerance of the measuring instrument ( $\pm 35 \text{ nT}$ ) was made, which is shown in Figure 8.

It can be observed that the differences between the measured and calculated magnetic field values are, except in specific points, within the tolerance range of the instrument. The difference between the theoretical and measured values within the contour of the loop is below 20% of the reading and the mean value is below 8%. Therefore, it can be concluded that the theoretical model for double loops developed in this paper predicts with a good precision the behavior of the magnetic field. In addition, different types of tests were also carried out with other types of loops, both single and double,

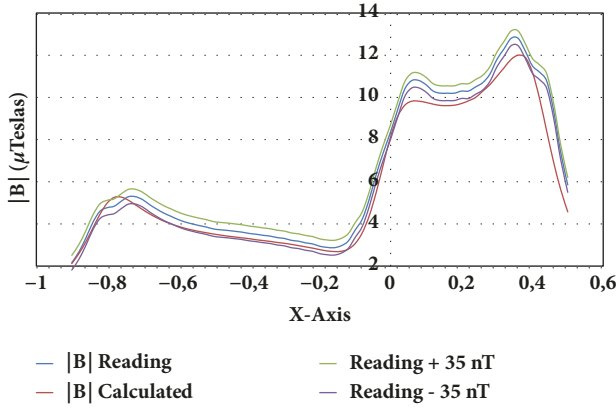


FIGURE 8: Calculated and measured values of the magnetic field  $|B|$ . The instrument tolerance is also considered.

varying the type and amplitude of the applied current, and very similar results were obtained.

#### 4. Methods for Inductance Calculation

Throughout time, various methods to calculate the inductance of magnetic loops according to different geometric configurations have been proposed [22–28], such as the Mills' method based on Grover's equations [22]. Most of the mathematical expressions for these calculations appear in classical texts [23] and based on these expressions, the inductance values presented by other different models of loops can be easily deduced.

However, the development of computer systems has allowed to implement numerical methods that make use of the intrinsic definition of the physical process of magnetic induction. In this regard, it would be convenient to include our previously presented work [25], in which the methods to calculate the inductance of a rectangular loop were analyzed and compared with other calculation techniques and real measures.

In this way, this time we will present three methods to calculate the inductance of the innovative double loops, since there are no studies about them. Therefore, these methods will be deeply analyzed and compared in order to know which method is more effective and if all of them are equally good. These three methods are as follows:

- (A) Electromagnetic Analysis Method
- (B) Numerical Integration Method
- (C) Mills and Grover's Method

(A) *Electromagnetic Analysis Method.* The first method to calculate the inductance of a double loop is based on the electromagnetic analysis, which considers the use of a numerical method that employs the expression of the magnetic field generated by a double loop. This means to carry out a study applied to the case of a double loop with the same structure as Figure 4.

The procedure starts by making use of the flux calculation, since all the loops work in the same way. However, in this case, the magnetic field and the flux will present some peculiarities.

The magnetic flux will be obtained as the integral of the product of the magnetic field by the differential surface all along the entire surface of the loop:

$$\emptyset = \int_S \vec{B}_K \cdot d\vec{S} \quad (22)$$

The expression of  $\vec{B}_K$  used in (22), which only taken into account the field in the Z direction, will be the same as in (20), and the differential surface can be easily replaced by the product of the differential length according to the X-axis and Y-axis as shown in the following:

$$\emptyset = \int_S \vec{B} d\vec{S} = \int_{-a}^d \int_{-b}^b B_K dy dx \quad (23)$$

To solve this expression, the integrals will be replaced by summations. For this, it is necessary to obtain the magnetic field in a series of points in space and consider a differential surface  $dydx$  around.

In this way, if we defined  $N_x$  as the number of points in which the magnetic field will be measured along the X-axis and  $N_y$  as the number of points in which the magnetic field will be measured along the Y-axis, the  $dx$  and  $dy$  differentials of (23) would be given by the following:

$$dx = \frac{d+a}{N_x}$$

$$dy = \frac{2b}{N_y} \quad (24)$$

Consequently, the total flux through the loop would be as shown in the following:

$$\emptyset = \sum_{n=1}^{N_x-1} \sum_{m=1}^{N_y-1} B_K(-a+ndx, -b+mdy, 0) f_x f_y dy dx \quad (25)$$

Summaries' limits have been designed to prevent the magnetic field measurements on the conductors, since at these points the value of  $B_K$  presents a singularity. The summation is extended to the rectangle defined by the points  $(-a+dx, d-dx)$  in the X-axis and  $(-b+dy, b-dy)$  in the Y-axis, but this causes an error in the measurement that has been tried to be solved by increasing the differential surface by 50% within the limits of the summation points. For this reason,  $f_x$  and  $f_y$  factors have been introduced [23]. The  $f_x$  factor takes a value 1 in all points except in those where  $n = 1$  or  $n = N_x - 1$  that has a value 1.5, and the  $f_y$  factor also takes a value 1 in all points except in those where  $m = 1$  or  $m = N_y - 1$  that has a value 1.5.

On the other hand, due to the abrupt change that appears in the  $B_K$  component of the magnetic field in the vicinity of the conductors, it is evident the importance of choosing the number of points  $N_x$  and  $N_y$ . In our previous article [25], it was shown that the optimal values of  $N_x$  and  $N_y$  to minimize

the error in the calculation of the inductance for a single rectangular loop were given by

$$\begin{aligned} N_x &= \frac{a+d}{3R_C} \\ N_y &= \frac{2b}{3R_C} \end{aligned} \quad (26)$$

where  $R_c$  is the radius of the conductor used to build the loop and  $a, d$  and  $2b$ , the dimensions of the loop shown in Figures 4 and 5. However, in this case, the space has been divided into three sections (two areas) as explained previously. For the positive region of the  $X$ -axis the flux is concatenated by  $N_1$  turns, and for the negative region of the  $X$ -axis, the flux is concatenated by  $N_1 \pm N_2$  turns as shown in Figure 5. The “+” sign would be used when the current goes through both loops in the same direction and the sign “-” when the current goes through the loops in opposite directions. Therefore, we could separate  $N_x$  into two sections as shown in Equation (27), which would represent the measured points, respectively, the negative and the positive ones at the  $X$ -axis.

$$\begin{aligned} N_{xa} &= \frac{a}{3R_C} \\ N_{xd} &= \frac{d}{3R_C} \end{aligned} \quad (27)$$

Finally, after all this mathematical and electromagnetic analysis, we could obtain the inductance of a double loop with dimensions  $a, d$  and  $2b$  and with  $N_1$  and  $N_1 \pm N_2$  turns respectively by the following expression:

$$\begin{aligned} L_0 &= \frac{1}{I} \left[ \sum_{n=1}^{N_{xa}-1} \sum_{m=1}^{N_y-1} (N_1 \pm N_2) B_K(-a+ndx, -b+mdy, 0) \right. \\ &\quad \cdot f_x f_y dy dx + \sum_{n=1}^{N_{xd}-1} \sum_{m=1}^{N_y-1} N_1 B_K(ndx, -b+mdy, 0) \\ &\quad \left. \cdot f_x f_y dy dx \right] \end{aligned} \quad (28)$$

In this expression,  $I$  represents the intensity used for the calculation of the magnetic field and the rest of values are known and have been described above. Nevertheless, it should be pointed out that the result of this first method will give the value of the inductance without considering the thickness of the loop, since this method is based only on the electromagnetic analysis of the magnetic field created by a double loop. Therefore, in this first method the spacing between the turns of the loop is considered null.

(B) *Numerical Integration Method.* After obtaining a first way to calculate the inductance of a double loop that does not take into account the spacing between turns, it seems reasonable that the second presented method does. These method, which apparently should provide more accurate

values, is the utilization of numerical integration techniques but considering the size and spacing between the turns of the loop ( $S_v$ ). However, on this occasion the calculation will be more complex than the last one, but these values are supposed to be much more real, since in reality the cables have a thickness that although it is minimal, it should be contemplated.

For the purpose of calculation mentioned, it is assumed an assembly in which the loops are stacked vertically. First, the larger  $N_1$  turns would be installed and after, over them, the smaller  $N_2$ , assuming that are equi-spaced a distance  $S_v$ . In this way, for each turn of the loop, the flux through it would be produced by the current that flows through the turn itself plus the flux generated by each of the other turns of the loop and which is concatenated by the one that is being analyzed.

The different flux components mentioned above will be represented by the terms  $\theta_{ijk}$ , where the subindex  $i$  indicates the type of loop which generates the field (1 Big, 2 Small), the subindex  $j$  indicates the type of loop which is crossed by the magnetic field (1 Big, 2 Small) and the subindex  $k$  indicates the distance between the loop that generates de field and the one which detects it. Hence, we can define the following terms:

- (i)  $\theta_{110}$  is the flux generated by one of the turns of the largest loops and which goes through them.
- (ii)  $\theta_{220}$  is the flux generated by one of the turns of the smallest loops and which goes through them.
- (iii)  $\theta_{11i}$  is the flux generated by a big turn which goes through the other big ones separated a distance  $iS_v$ .
- (iv)  $\theta_{12j}$  is the flux generated by a big loop which goes through the other small ones separated a distance of  $jS_v$  from the turn that has generated the flux.
- (v)  $\theta_{22k}$  is the flux generated by a small turn which goes through the other small ones separated a distance of  $kS_v$ .
- (vi)  $\theta_{21l}$  is the flux generated by a small loop which goes through the other big ones separated a distance  $lS_v$  from the turn that has generated the flux.
- (vii)  $N_{min}$  will be the minimum value between  $N_1$  and  $N_2$  and  $N_{max}$  will be the maximum value between  $N_1$  and  $N_2$ .

With this nomenclature, the inductance of the double loop would be given by the following:

$$\begin{aligned} L_{IIC} &= \frac{1}{I} \left[ \sum_{i=0}^{N_1} (N_1 - i) \theta_{11i} \pm \sum_{i=0}^{N_2} (N_2 - i) \theta_{22i} \right. \\ &\quad + \sum_{i=1}^{N_{min}} i (\theta_{12i} \pm \theta_{21i}) + \sum_{i=N_{min}+1}^{N_{max}} N_{min} (\theta_{12i} \pm \theta_{21i}) \\ &\quad \left. + \sum_{i=N_{max}+1}^{N_1+N_2-1} (N_1 + N_2 - i) (\theta_{12i} \pm \theta_{21i}) \right] \end{aligned} \quad (29)$$

The “+” sign would be used when the current goes through both loops in the same direction while the sign “-” would

be used when the current goes through the loops in opposite directions. In any case, the fluxes described and shown in (29) are given by the following:

$$\begin{aligned}
\emptyset_{11i} &= \left[ \sum_{n=1}^{N_{x1}-1} \sum_{m=1}^{N_{y1}-1} B_{KR1} \left( -\frac{d+a}{2} + ndx, -b + mdy, i \cdot S_v \right) \right. \\
&\quad \left. \cdot f_x f_y dy dx \right] \\
\emptyset_{22i} &= \left[ \sum_{n=1}^{N'_{x1}-1} \sum_{m=1}^{N_{y1}-1} B_{KR2} \left( -\frac{a}{2} + ndx, -b + mdy, i \cdot S_v \right) \right. \\
&\quad \left. \cdot f_x f_y dy dx \right] \\
\emptyset_{12i} &= \left[ \sum_{n=1}^{N'_{x1}-1} \sum_{m=1}^{N_{y1}-1} B_{KR1} \left( -\frac{a}{2} + ndx, -b + mdy, i \cdot S_v \right) \right. \\
&\quad \left. \cdot f_x f_y dy dx \right] \\
\emptyset_{21i} &= \left[ \sum_{n=1}^{N_{x1}-1} \sum_{m=1}^{N_{y1}-1} B_{KR2} \left( -\frac{d+a}{2} + ndx, -b + mdy, i \cdot S_v \right) \right. \\
&\quad \left. \cdot f_x f_y dy dx \right]
\end{aligned} \tag{30}$$

In  $\emptyset_{11i}$ ,  $B_{KR1}(x, y, z)$  is the magnetic field component along the Z-axis generated by a large turn, extending from  $-a$  to  $+d$  along the X-axis and from  $-b$  to  $+b$  along the Y-axis at the point of space  $(x, y, z)$ .

In  $\emptyset_{12i}$ ,  $B_{KR1}(x, y, z)$  is also the magnetic field component along the Z-axis generated by a large turn, extending from  $-a$  to  $+d$  along the X-axis and from  $-b$  to  $+b$  along the Y-axis at the point of space  $(x, y, z)$ .

In  $\emptyset_{22i}$ ,  $B_{KR2}(x, y, z)$  is the magnetic field component along the Z-axis generated by a small turn, extending from  $-a$  to  $0$  along the X-axis and from  $-b$  to  $+b$  along the Y-axis at the point of space  $(x, y, z)$ .

In  $\emptyset_{21i}$ ,  $B_{KR2}(x, y, z)$  is also the magnetic field component along the Z-axis generated by a small turn, extending from  $-a$  to  $0$  along the X-axis and from  $-b$  to  $+b$  along the Y-axis at the point of space  $(x, y, z)$ .

The values used in (29) and (30) ( $N_{x1}$ ,  $N_{y1}$ ,  $dx$ ,  $dy$ ,  $f_x$ ,  $f_y$ ) are the same ones used to calculate the previous inductance and  $N'_{x1}$  takes the following value:

$$N'_{x1} = \frac{a}{3R_C} \tag{31}$$

As it can be seen, this method seems much more accurate than the previous one, but it is true that there is a high amount of operations and summations to perform, which will make it more difficult to implement and with higher computational

cost. Therefore, taking into account the fact that the first method did not consider spacing between the turns of the loop, which is not physically correct, and that the second method, although it does, is computationally complicated because of the large number of operations and summations, it leads us to think of a third method that also considers spacing but is much simpler to implement.

(C) *Mills and Grover's Method.* In order to calculate the inductance of a double loop, Mills and Grover's method will be proposed. As said above, in this third and last method it will be taken into account again that the size of the conductors prevents all turns from being in the same coordinate Z. To consider this phenomenon, studies such as Mills' emerged [22, 28], from which new expressions of inductance were deduced.

When working with double loops, the self-inductance of the  $N_1$  turns of the loop and, over them, the  $N_2$  turns, equally spaced a distance  $S_v$ , is represented by the following:

$$\begin{aligned}
L_T &= N_1 L_{10} \pm N_2 L_{20} + \sum_{n=1}^{N_1-1} (N_1 - n) M_{11}(nS_v) \\
&\quad \pm \sum_{n=1}^{N_2-1} (N_2 - n) M_{22}(nS_v) \\
&\quad + \sum_{n=1}^{N_1} \sum_{m=1}^{N_2} (M_{12}(S_v(N_1 + m - n)) \\
&\quad \pm M_{21}(S_v(N_1 + m - n)))
\end{aligned} \tag{32}$$

where

- (i)  $L_{10}$  is the self-inductance of a rectangular loop with only one large-size turn  $(a + d) \times 2b$ ;
- (ii)  $L_{20}$  is the self-inductance of a rectangular loop with also only one small-size turn  $(a \times 2b)$ ;
- (iii)  $M_{11}(nS_v)$  is the mutual inductance between two turns of a rectangular large loop separated between them at a distance of  $nS_v$ ;
- (iv)  $M_{22}(nS_v)$  is the mutual inductance between two turns of a rectangular small loop separated between them at a distance of  $nS_v$ ;
- (v)  $M_{12}(S_v(N_1 + m - n))$  are the mutual inductances between a big-size turn and a small-size turn separated at a distance of  $S_v(N_1 + m - n)$ .

It must be noted that the above-mentioned parameters  $L_{10}$  and  $L_{20}$  are obtained as the sum of the internal and external inductance of the conductors that constitute the loop as follows:

$$\begin{aligned}
L_0 &= L_{0i} + L_{0e} \\
L_{10i} &= 2(a + d + 2b) L_i \\
L_{20i} &= 2(a + 2b) L_i
\end{aligned} \tag{33}$$

where  $L_i$  is the inductance per unit length, which must consider the relationship between the inductance at a certain

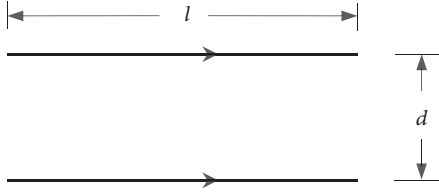


FIGURE 9: Features of two ideal parallel conductors of no straight section for measuring mutual induction.

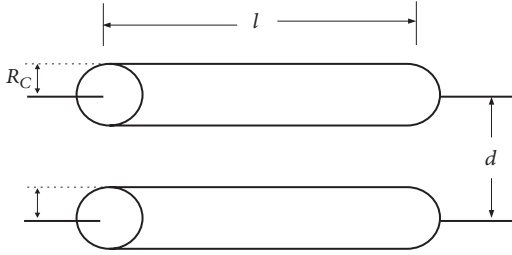


FIGURE 10: Features of two parallel conductors to measure the mutual induction.

frequency  $L_i$  and the inductance at low frequency  $L_{i0}$ . In order to carry out these operations, we will use Johnson's studies [23]. In this manner,

$$L_i = L_{i0} \cdot \frac{4}{q} \left[ \frac{bei(q) \times bei'(q) + ber(q) \times ber'(q)}{(bei'(q))^2 + (ber'(q))^2} \right] \quad (34)$$

where  $bei(q)$ ,  $ber(q)$ ,  $bei'(q)$ , and  $ber'(q)$  are the imaginary and real parts of the Bessel function of first order and their derivatives, which are necessary for the calculations when this method is applied. On the other hand, the inductance per unit length at a low frequency is given by (35), but for copper conductors it takes a value of  $0.5 \cdot 10^{-7} H/m$ :

$$L_{i0} = \frac{\mu_0 \mu_r}{8\pi} \quad (35)$$

To obtain  $L_{oe}$  [22–27], we focus on the mutual inductance of a pair of parallel conductors, whose expression is:

$$M(l, d) = \pm \frac{\mu_0 l}{2\pi} \left\{ \ln \left[ \frac{l}{d} + \sqrt{1 + \left(\frac{l}{d}\right)^2} \right] - \sqrt{1 + \left(\frac{d}{l}\right)^2} + \frac{d}{l} \right\} \quad (36)$$

As seen in Figure 9,  $l$  is the length of the filaments and  $d$  is the separation between them (both quantities expressed in meters), which results in an inductance expressed in Henrys. This expression takes a positive sign when the current in both cables has the same direction and takes a negative sign when the current has opposite directions.

In addition, it is known that the external inductance of a pair of parallel conductors with the dimensions shown in Figure 10 is given by

$$L_p = L_1 - M_{12} + L_2 - M_{21} \quad (37)$$

$L_1$  and  $L_2$  are the self-inductances of the simple conductors and  $M_{12}$  and  $M_{21}$  are the mutual inductance measures between the centers of the conductors, assuming a uniform current distribution throughout the cross section of the conductor. Mutual inductances have been considered to have a negative sign as it has been assumed that the current in the two conductors have opposite directions. Therefore, if both conductors have the same dimensions:

$$L = L_1 = L_2 \text{ and} \quad (38)$$

$$M = M_{12} = M_{21}$$

Thus:

$$L_p = 2(L - M) \quad (39)$$

The external self-inductance of a conductor is obtained thanks to a method in which the conductor is replaced with two conductors with a null straight section separated by a distance equal to the radius of the conductor. In this way

$$L_p = 2(M(l, R_C) - M(l, d)) \quad (40)$$

In addition, the inductance of a rectangular loop with a single turn is given by the sum of the inductance of two pairs of parallel conductors as follows:

$$L_{0e} = L_{p1} + L_{p2}$$

$$L_{0e} = 2[M_1(l_1, R_C) - M_1(l_1, l_2) + M_2(l_2, R_C) - M_2(l_2, l_1)] \quad (41)$$

where  $l_1 = a + d$  and  $l_2 = 2b$  for the big loop and  $l_1 = a$  and  $l_2 = 2b$  for the small loop.

As it can be deduced from this expression, the external inductance of a rectangular loop with one turn is equal to the mutual inductance of two identical coaxial rectangular loops separated by a distance equal to the radius of the conductor. In this way, the mutual inductance of two parallel rectangular loops as shown in Figure 11 can be obtained from mutual inductances between parallel conductors.

Therefore, the mutual inductance between the two rectangular loops with the same dimensions as shown in Figure 11 may be expressed as follows:

$$M = -2[M_{13}(A, \sqrt{H^2 + B^2}) - M_{11}(A, H) + M_{24}(B, \sqrt{H^2 + A^2}) - M_{22}(B, H)] \quad (42)$$

In the above expression, the terms  $M_{ij}$  represent the mutual inductance between the segment  $i$  of the bottom loop and the segment  $j$  of the top loop. The reason to multiply the expression by two is because the mutual inductances are all symmetric, that is, for all  $i$  and all  $j$ ,  $M_{ij} = M_{ji}$ .

On the other hand, to calculate the mutual inductance between two parallel loops with different dimensions, Grover's equations must be used again, since they provide the mutual inductance between two parallel straight conductors as shown in Figure 12.

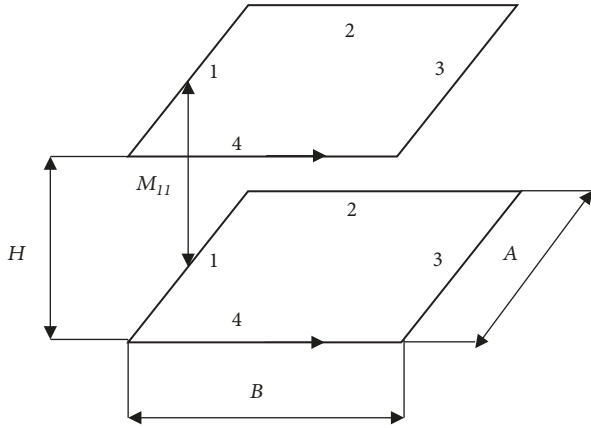


FIGURE 11: Geometry for calculating the mutual inductance between two parallel and coaxial rectangular loops with the same dimensions.

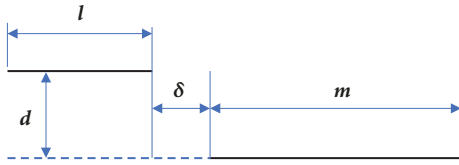


FIGURE 12: Disposition of two parallel straight conductors.

According to Grover's formula, the mutual inductance between two parallel conductors with sizes  $l$  and  $m$  spaced a distance  $d$  and displaced at a distance  $\delta$  is given by

$$M_G(l, m, d, \delta) = \frac{\mu_0}{4\pi} \left[ \alpha \sinh^{-1} \left( \frac{\alpha}{d} \right) - \beta \sinh^{-1} \left( \frac{\beta}{d} \right) - \gamma \sinh^{-1} \left( \frac{\gamma}{d} \right) + \delta \sinh^{-1} \left( \frac{\delta}{d} \right) - \sqrt{\alpha^2 + d^2} - \sqrt{\beta^2 + d^2} + \sqrt{\gamma^2 + d^2} - \sqrt{\delta^2 + d^2} \right] \quad (43)$$

where

$$\begin{aligned} \alpha &= l + m + \delta, \\ \beta &= l + \delta, \\ \gamma &= m + \delta \end{aligned} \quad (44)$$

It should be pointed out that if the two conductors overlap partially or totally, the parameter  $\delta$  will have negative values.

In any case, from all these expressions it is finally possible to obtain the inductance between two parallel rectangular loops with different dimensions as shown in Figure 13, which is simply another way of seeing Figures 4 and 5.

Therefore, the mutual inductance between the two parallel loops is finally obtained as a sum of the mutual inductances of the parallel conductors where the terms  $M_{ij}$  represent mutual inductances between two parallel rectilinear conductors with the same dimensions, and the terms  $M_{Gij}$  represent the mutual inductances between two parallel rectilinear

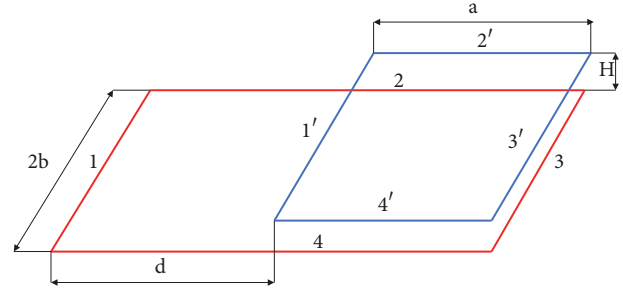


FIGURE 13: Disposition of two parallel loops of different dimensions.

conductors with different dimensions. This is shown in the following:

$$\begin{aligned} M_{EE}(d, a, 2b, H) &= M_{11} \left( 2b, \sqrt{d^2 + H^2} \right) \\ &\quad - M_{13} \left( 2b, \sqrt{(d+a)^2 + H^2} \right) \\ &\quad - M_{31} \left( 2b, \sqrt{a^2 + H^2} \right) + M_{33} (2b, H) \\ &\quad + M_{G22} (d+a, a, h, -a) \\ &\quad - M_{G24} (d+a, a, \sqrt{4b^2 + H^2}, -a) \\ &\quad - M_{G42} (d+a, a, \sqrt{4b^2 + H^2}, -a) \\ &\quad + M_{G44} (d+a, a, h, -a) \\ &= M_{11} \left( 2b, \sqrt{d^2 + H^2} \right) \\ &\quad - M_{13} \left( 2b, \sqrt{(d+a)^2 + H^2} \right) \\ &\quad - M_{31} \left( 2b, \sqrt{a^2 + H^2} \right) + M_{33} (2b, H) \\ &\quad + 2M_{G22} (d+a, a, h, -a) \\ &\quad - 2M_{G24} (d+a, a, \sqrt{4b^2 + H^2}, -a) \end{aligned} \quad (45)$$

Although this last equation may seem complicated and with a large number of operations, it should not be forgotten that in none of the previous expressions there are integrals or summations. The maximum operations that appear are square roots and trigonometric functions. Therefore, it apparently seems to be the method that best behaves computationally. Moreover, this also considered spacing between the turns of the loop as the second one.

Thus, once all methods have been presented, the inductance values obtained are going to be compared to each other to verify the similarity between them and know which the best methods are and which are not.

## 5. Results and Discussion

After making the description and performing the analysis of the three methods, the first thing that stands out is that there are two methods that consider the spacing between the turns ( $S_v$ ) and one which does not. For that reason, what would be expected at first sight is that the accuracy and complexity of the two methods which do consider this are greater than the method which does not. Therefore, the inductance values obtained by using the electromagnetic analysis method should provide different values than the other ones, but a simple explanation for this phenomenon would be the fact of not having considered the flux lines that are lost between the loops because of the fact that they have a real thickness which is not zero.

To check all of the above, various test related to the inductance values of the different methods and types of loops were performed and are presented below. In fact, it was studied the effect of increasing the number of turns in a single and in a double loop and the effect of changing the dimensions of a double loop.

*5.1. How the Number of Turns Affects the Value of the Inductance of a Single Loop.* For the purpose of this study, a single  $2 \times 2$  loop located and centered in the  $XY$  plane with a cable radius of  $0.75\text{mm}$  and a turn spacing of  $1.9\text{mm}$  was used. In this first test, the number of turns of the loop was gradually increased to see the effect that it has on the value of its inductance. With the nomenclature described in the paper, the characteristics of this loop were as follows:

- (i)  $a = 1 \text{ meter}$
- (ii)  $b = 1 \text{ meter}$
- (iii)  $d = 1 \text{ meter}$
- (iv)  $N_1 = \text{From } 1 \text{ to } 7$
- (v)  $N_2 = 0$

As mentioned, in the ideal case it would be expected for the three methods to provide similar results, but it is clearly observed in Figure 14(a) that there are two methods that are practically identical, and one method whose results are far from the other ones. Therefore, the first point to emphasize is that the Mills and Grover's method and the numerical integration method, those that consider the separation between turns, provide good and identical results, while the method based on the electromagnetic analysis begins to fail when the turns increase.

This means that the more turns the loops have, the more different the results are, because the error of not considering separation between turns increases for each turn.

*5.2. How the Number of Turns Affects the Value of the Inductance of a Double Loop.* The next test was the same as the previous one but instead of working with a single loop, we will work with a double loop. This time, it was a double  $2 \times 2$  loop formed by an external loop of  $N_1$  turns located and centered in the  $XY$  plane and a smaller one of  $N_2$  turns located in the half-plane of the negative values of  $X$ , both

with a cable radius of  $0.75\text{mm}$  and a turn spacing of  $1.9\text{mm}$ . In the previous analysis, only the number of turns  $N_1$  was varied since it was a single loop and  $N_2 = 0$ . However, as we were working with a double loop, to check the effect of increasing the number of turns, the value of  $N_1$  was kept fixed and  $N_2$  was the value that we were gradually increasing. In this way, with the nomenclature described in the paper, the characteristics of this double loop were as follows:

- (i)  $a = 1 \text{ meter}$
- (ii)  $b = 1 \text{ meter}$
- (iii)  $d = 1 \text{ meter}$
- (iv)  $N_1 = 3$
- (v)  $N_2 = \text{From } 1 \text{ to } 7$

The result obtained was really similar to the previous one. As it can be seen in Figure 14(b), the two methods that consider spacing provided practically identical values, while the electromagnetic analysis method, as it does not, provided different values, this time greater. The fact that the results were even greater is because as we had concluded before, the more turns the loops have, the more different the results are, and there are more turns in a double loop ( $N_1$  in the first loop and  $N_1 + N_2$  in the second one) than in a single one (only  $N_1$ ). Thus, at this point we could already begin to draw conclusions, but in order to make a study as rigorous as possible, we will show more results from our analysis.

*5.3. How the Dimensions of the Loop Affect the Value of the Inductance of a Double Loop.* Once we had analyzed how the number of turns affects the inductance value, in the two remaining experiments we analyzed what happens when varying the dimensions of the loops. For this purpose, we worked with a double loop formed by  $N_1$  large turns, centered with respect to the  $Y$ -axis, extending from  $-a$  to  $+d$  along the  $X$ -axis, and  $N_2$  small turns, also centered with respect to the  $Y$ -axis, extending from  $-a$  to  $0$  along the  $X$ -axis. Both had a cable radius of  $0.75\text{mm}$  and a turn spacing of  $1.9\text{mm}$ . In this way, the number of turns was kept fixed and the value that we varied was the length  $a$ , which means increasing the length of the smallest loop, which has  $N_2$  turns and is located in the negative half-plane. In addition, it should be noted that this fact also increases the length of the biggest loop, since its dimensions are  $(a + d) \times 2b$ . Then, with the nomenclature described in the paper, the characteristics of this loop were as follows:

- (i)  $a = \text{From } 1 \text{ to } 10 \text{ meters}$
- (ii)  $b = 1 \text{ meter}$
- (iii)  $d = 1 \text{ meter}$
- (iv)  $N_1 = 3$
- (v)  $N_2 = 2$

In Figure 14(c) it can be observed very clearly that although the trend of the three methods was the same, the results were different. Mills and Grover's method as well as the numerical integration one had a practically linear relationship between

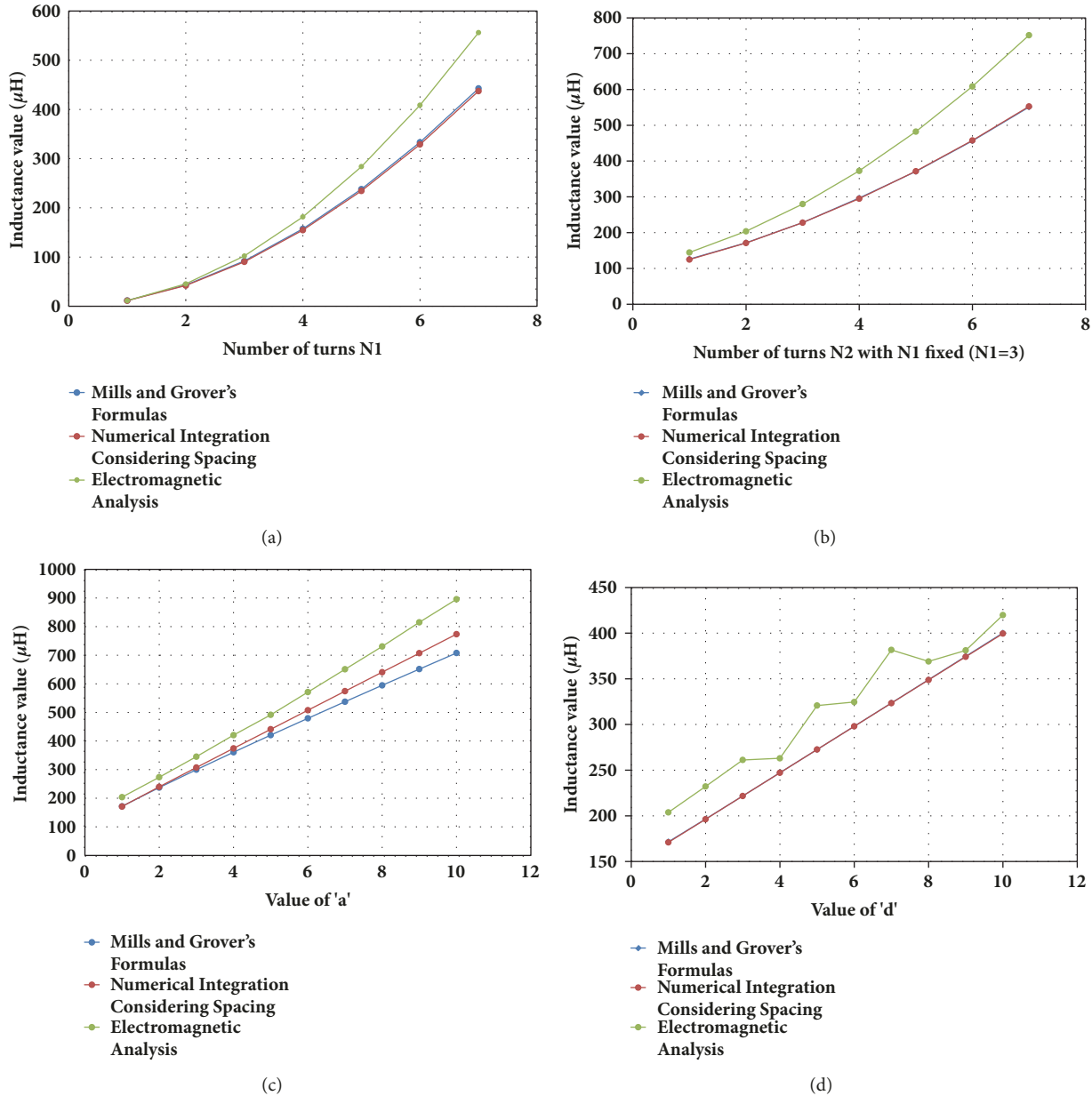


FIGURE 14: Inductance values. (a) When increasing the number of turns in a single loop. (b) When increasing the number of turns in a double loop. (c) When increasing the length of “a” in a double loop. (d) When increasing the length of “d” in a double loop.

the increase of  $a$  and the increase of the inductance. However, it is noted that the first method, which had extracted its equations from the analysis of the electromagnetic field without considering spacing, gave results distant from the real ones from the beginning, being this error greater as the length of  $a$  is bigger.

On the other hand, after analyzing what happens when the length of  $a$  is increased, it was analyzed what happens precisely if we increase the length of  $d$ , with whose variation we only be modify the length of the largest loop. The double loop was again formed by  $N_1$  large turns, centered with respect to the  $Y$ -axis, extending from  $-a$  to  $+d$  along the  $X$ -axis, and  $N_2$  small turns, also centered with respect to the

$Y$ -axis and extending from  $-a$  to  $0$  along the  $X$ -axis. Both had a cable radius of  $0.75\text{mm}$  and a turn spacing of  $1.9\text{mm}$ . The number of turns was kept fixed again and the value that we varied was  $d$ . In this manner, with the nomenclature described in the paper, the characteristics of this loop were as follows:

- (i)  $a = 1$  meter
- (ii)  $b = 1$  meter
- (iii)  $d =$  From 1 to 10 meters
- (iv)  $N_1 = 3$
- (v)  $N_2 = 2$

In this test, it was seen how two methods followed the same trend again, providing almost the same results, but the other one did not behave properly. However, in Figure 14(d) it is clear that Mills and Grover's method and the method of numerical integration provide exactly the same values and the electromagnetic analysis method does not.

Therefore, after analyzing the previous results, we could conclude that of the three methods proposed, the electromagnetic method could be useful for very thin conductors with little separation between them and for complex geometries in which Mills and Grover can not be used, as it only serves for parallel and perpendicular conductors. When it was tried to increase the turns of the loop, it was the only one that differed from the rest. On the other hand, when the length of the loop was increased, it was also evident that this method did not behave correctly. For this reason, we can affirm that although it is a valid method and can give us an approximation if the separation between turns is big, it should be only used as a reliable source if that separation is minimal.

Regarding the two remaining methods, it must be noted that both offer good and similar results as it can be seen in Figures 14(a), 14(b), 14(c) and 14(d), but in the case of having to opt for one of them, we must emphasize that the numerical integration method carries a much higher computational cost than the Mills and Grover's one. In fact, it is clear by observing Figure 14 that this method had the best behavior in every of the cases. Then, we could conclude that because of its low computational cost and extreme accuracy, Mills and Grover's method would be the best way of calculating the inductance of a double magnetic loop, which is why it will be the one that we will use in our simulation programs.

## 6. Conclusions

This article is aimed to be a presentation of the double loop, where geometry, construction, operating mode and three possible ways to calculate its inductance have been explained. After presenting these three above-mentioned methods, an analysis has clarified that if precision is required, Mills and Grover's method or the numerical integration method must be used, as they both take into account the separation between turns, although we recommend to choose the first one because of its low computational cost.

In future papers, we will focus more closely on the advantages offered by using this type of loops, what will help to understand the need and importance of this paper. It will focus on the new vehicle magnetic profiles, the parameters that can be extracted from them and the benefits of using them in comparison with the conventional loops.

The reality is that magnetic loops, despite being from the eighties, are still the most used technology to capture data from traffic. For that reason, we must improve the existing infrastructure and provide this sensor with greater potential and reliability.

## Data Availability

The data used to support the findings of this study are included within the article.

## Conflicts of Interest

The authors declare that they have no conflicts of interest.

## References

- [1] R. L. Anderson, "Electromagnetic loop vehicle detectors," *IEEE Transactions on Vehicular Technology*, vol. VT-19, no. 1, pp. 23–30, 1970.
- [2] M. J. Caruso, T. Bratland, C. H. Smith, and R. Schneider, "A new perspective on magnetic field sensing," *Sensors (Peterborough, NH)*, vol. 15, no. 12, pp. 34–46, 1998.
- [3] L. A. Klein, D. R. P. Gibson, and M. K. Mills, *Traffic Detector Handbook*, vol. FHWAHRT-06-108, Federal Highway Administration, U.S. Department of Transportation, 2006.
- [4] N. L. Nihan, "Evaluation of forced flows on freeways with single-loop detectors," *Journal of Advanced Transportation*, vol. 34, no. 2, pp. 269–296, 2000.
- [5] H. Wang, Z. Li, D. Hurwitz, and J. Shi, "Parametric modeling of the heteroscedastic traffic speed variance from loop detector data," *Journal of Advanced Transportation*, vol. 49, no. 2, pp. 279–296, 2015.
- [6] M. Bugdol, Z. Segiet, M. Krecichwost, and P. Kasperek, "Vehicle detection system using magnetic sensors," *Transp. Problems*, vol. 9, no. 1, pp. 49–60, 2014.
- [7] F. C. Nemtanu, J. Schlingensiepen, D. Buretea, and V. Iordache, "Mobility as a service in smart cities," in *ICEIRD 2016 – Responsible Entrepreneurship Vision, Development and Ethics*, pp. 425–435, 2016.
- [8] T. V. Mathew, "Transportation systems engineering," in *IIT Bombay, Chapter 9– Intrusive Technologies*, School: Jessore Science & Technology University, Bangladesh, 2014.
- [9] S. Meta and M. G. Cinsdikici, "Vehicle-classification algorithm based on component analysis for single-loop inductive detector," *IEEE Transactions on Vehicular Technology*, vol. 59, no. 6, pp. 2795–2805, 2010.
- [10] D. Guilbert, S.-S. Ieng, C. L. Bastard, and Y. Wang, "Robust blind deconvolution process for vehicle reidentification by an inductive loop detector," *IEEE Sensors Journal*, vol. 14, no. 12, pp. 4315–4322, 2014.
- [11] L. Bhaskar, A. Sahai, D. Sinha, G. Varshney, and T. Jain, "Intelligent traffic light controller using inductive loops for vehicle detection," in *Proceedings of the 1st International Conference on Next Generation Computing Technologies, NGCT 2015*, pp. 518–522, India, September 2015.
- [12] J. Gadjia, R. Sroka, M. Stencil et al., *Measurements of Road Traffic Parameters*, Publishing House PWN, 2015.
- [13] L. A. Klein, *Sensors Technologies and Data Requirements for ITS*, Artech House, 2011.
- [14] Z. Marszalek, R. Sroka, and T. Zeglen, "Inductive loop for vehicle axle detection from first concepts to the system based on changes in the sensor impedance components," in *Proceedings of the 2015 20th International Conference on Methods and Models in Automation and Robotics (MMAR)*, pp. 765–769, Miedzyzdroje, Poland, August 2015.
- [15] Z. Marszalek, R. Sroka, and T. Zeglen, "Multi-frequency conditioning system of the inductive loop sensor — Simulation investigations," in *Proceedings of the 2017 22nd International Conference on Methods and Models in Automation and Robotics (MMAR)*, pp. 889–893, Miedzyzdroje, Poland, August 2017.

- [16] D. S. García, J. T. Arjona, and J. M. M. García, *Cuaderno Tecnológico de la PTC – Sistemas de Adquisición de Información de Tráfico: Estado Actual y Futuro*, Plataforma Tecnológica Española de la Carretera (PTC), Madrid, 2011.
- [17] A. L. J. Ortega, *OEP 2013. Especialidad: Gestión Técnica del Tráfico 2011*, Chapter 30, 2013.
- [18] S. S. M. Ali, B. George, L. Vanajakshi, and J. Venkatraman, “A multiple inductive loop vehicle detection system for heterogeneous and lane-less traffic,” in *Proceedings of the IEEE Transactions on Instrumentation and Measurement*, vol. 61, pp. 1353–1360, 2012.
- [19] J. H. Arroyo-Núñez, *Estudio del Comportamiento Magnético de Espiras Rectangulares para la Transmisión de Información de Corto Alcance en Sistemas Inteligentes de Transporte [Ph.D. thesis]*, Dept. of Electrical Engineering University Politécnica València, Valencia, 2016.
- [20] G. TurnBull, “Maxwell’s Equations,” in *Proceedings of the IEEE*, vol. 101, pp. 0018–9219, 2013.
- [21] S. Errede, “Lecture Notes 16. The magnetic vector potential,” *Physics 435 EM Fields & Sources I*, 2007.
- [22] M. Mills, “Self inductance formulas for multi-turn rectangular loops used with vehicle detectors,” in *Proceedings of the 33rd IEEE Vehicular Technology Conference*, pp. 65–73, May 1983.
- [23] E. B. Rosa and F. W. Grover, “Formulas and tables for the calculation of mutual and self-inductance (Revised),” *Bulletin of the Bureau of Standards*, vol. 8, no. 1, p. 1, 1912.
- [24] F. C. Nemptanu, I. M. Costea, and L. G. Obreja, “Model of intelligent traffic sensors — Application in hardware in the loop,” in *Proceedings of the 2017 40th International Spring Seminar on Electronics Technology (ISSE)*, pp. 1–5, Sofia, Bulgaria, May 2017.
- [25] A. Mocholí-Salcedo, J. H. Arroyo-Núñez, M. Víctor, J. Gumersindo, and A. Arroyo-Núñez, “Magnetic field generated by the loops used in traffic control systems,” in *Proceedings of the IEEE Transactions on Intelligent Transportation Systems*, 2017.
- [26] M. Misakian, “Equations for the magnetic field produced by one or more rectangular loops of wire in the same plane,” *Journal of research of the National Institute of Standards and Technology*, vol. 105, no. 4, pp. 557–564, 2000.
- [27] Y. Niwa, “A study of coils wound on rectangular frames with special reference to the calculation of inductance,” *Researches of the Electrotechnical Laboratory*, vol. 141, 1924.
- [28] F. W. Grover, *Inductance Calculations: Working Formulas and Tables*, New York, NY, USA, 1962.

